Quantitative analysis of sub-catchment scale erosion-sedimentation dynamics in a grassed buffer zone using hyper-resolution soil loss modeling in a Hungarian hilly arable environment

Authors: Z. Szenek[1], D. Szám[1], Cs. Centeri[2], G. Milics[3]
[1]Duo Sense Ltd., 36. Szélmalom street, Kecskemét, H-6000, Hungary
[2]Hungarian University of Agriculture and Life Sciences (MATE), Institute for Wildlife Management and Nature Conservation, 1. Páter K. Street, Gödöllő, H-2100, Hungary
[3]Hungarian University of Agriculture and Life Sciences (MATE), Institute of Agronomy, Department of Precision Agriculture and Digital Farming, 1. Páter K. Street, Gödöllő, H-2100, Hungary
Corresponding author: centeri.csaba@uni-mate.hu

Abstract

Soil erosion represents one of the most severe environmental and economic risks in arable crop production, leading to the irreversible degradation of the topsoil layer. The primary objective was to validate the real-world applicability and academic scientific merit of process-based soil conservation planning using a multi-tiered validation workflow. This research also aims to provide a quantitative analysis of the sediment retention capacity of a grassed buffer strip installed within an erosion rill, utilizing 1×1 m resolution soil loss modeling.

The methodological base of the study was the Unit Stream Power-based Erosion Deposition (USPED) model. The application of USPED enabled overcoming the classical USLE limitations by accounting for the impact of rill erosion during sediment transport modeling. The modeling framework utilized a high-precision Digital Elevation Model (DEM) generated photogrammetrically via UAV. Flow accumulation calculations identified the primary rill erosion pathways where the grassed strip was strategically positioned. The sub-catchment area was delineated using the Watershed geoprocessing tool, upon which a 1×1 m grid was superimposed to calculate the USPED factors at the cell level (Equation 1).

The soil erodibility factor (K-factor) was derived from laboratory measurements of samples taken from the upper genetic horizons of two soil profile excavations located in the erosion and accumulation zones, rather than using tabular estimates. Saturated hydraulic conductivity was determined via infiltrometer measurements, followed by the application of the modern EPIC (Erosion-Productivity Impact Calculator) algorithm for K-factor calculation. For the slope length and steepness factor (LS-factor), a pixel-level (0.43 × 0.43 m) outlier detection algorithm was executed on the DEM point cloud to ensure data integrity. The rainfall erosivity factor (R-factor) was calculated using the 1991–2020 average annual precipitation data from the Hungarian Meteorological Service. The cover-management factor (C-factor) was derived from the field's characteristic crop rotation, while the support practice factor (P-factor) followed the Wischmeier-Smith approach.

The authors are solely responsible for the content of this paper, which is not a refereed publication. Citation of this work should state that it is from the Proceedings of the 17th International Conference on Precision Agriculture and 11th Brazilian Congress on Precision and Digital Agriculture. EXAMPLE: Last Name, A. B. & Coauthor, C. D. (2026). Title of paper. In Proceedings of the 17th International Conference on Precision Agriculture and 11th Brazilian Congress on Precision and Digital Agriculture (unpaginated, online). Monticello, IL: International Society of Precision Agriculture and Brazilian Congress on Precision and Digital Agriculture.

Field surveys validated the model predictions: a truncated profile was identified in the erosion zone (A+B horizons thickness: 0.4 m), while a 1.4 m deep sedimented layer (A+B horizons) was found in the accumulation zone. Infiltrometer tests revealed extremely poor infiltration in the erosion zone (Wischmeier permeability class: 6) and moderate rates in the accumulation zone (Wischmeier permeability class: 3). Evaluating the 3.51 ha sub-catchment area across 35,922 individual cells, the potential soil loss without protection was calculated at 85.98 t ha^{-1} (24.50 t ha^{-1} yr^{-1}). With the integration of a 4.5 m wide grassed strip - which exhibits a 25.4% deposition efficiency based on the exponential saturation model - the sub-catchment achieved a sediment retention performance of 21.84 t ha^{-1} for 2-year return period rainfall events, and 52.41 t ha^{-1} for extreme events with a 20-year return frequency. Spearman correlation analysis indicated a strong positive relationship (R=0.86) between soil loss and flow accumulation across all cells. These results consistently demonstrate that Nature-based Solutions (NbS) supported by hyper-resolution GIS planning can significantly mitigate soil degradation with minimal land withdrawal.

Keywords: *Grassed buffer strips, Hyper-resolution soil loss modeling, Nature-based Solutions (NbS), Sediment retention dynamics, USPED model*

Introduction

Soil erosion is one of the most critical environmental and economic threats to arable crop production, leading to the irreversible degradation of the topsoil layer. On a global scale, the rate of soil degradation far exceeds the natural pace of soil formation, which poses a direct threat to food security, according to reports by the Food and Agriculture Organization (FAO). Altered rainfall dynamics resulting from climate change—particularly increased intensity, extreme flash floods, and the subsequent high-volume runoff events—induce severe erosional damage (Centeri et al. 2019). This process is frequently irreversible. It deteriorates soil water management, reduces crop yields, and causes the eutrophication of recipient water bodies due to washed-out sediment.

Although modern precision agriculture has successfully standardized variable-rate nutrient and chemical application, a technological gap remains. Automated, high-resolution spatial engineering solutions for precision soil conservation are still almost entirely missing from agricultural management (Milics 2015).

One of the aims of this study is to provide a quantitative analysis of the sediment retention capacity of a grassed buffer strip installed within an active erosion rill, utilizing 1×1 m resolution soil loss modeling. Nature-based Solutions (NbS), such as grassed buffer zones, demonstrate excellent efficiency in reducing runoff velocity and trapping suspended solids. However, their planning and implementation often ignore actual runoff patterns. This research establishes a framework to address this issue by developing and presenting a high-resolution (1×1 m) geospatial workflow. This pipeline integrates UAV photogrammetry, process-based USPED modeling, and in situ pedological and hydraulic field validation to measure the sediment retention efficiency of a precision grassed strip designed for a hilly Hungarian arable environment.

The investigation was conducted on an 11.85-hectare intensively managed arable field located in the southern terminal basin of the Vértestolna Basin (18,4437339°E 47,6173908°N). The climate of the area is moderately cool and dry, with an unevenly distributed annual precipitation ranging between 0.55 and 0.62 m. The topography is characterized by farming on valley floors, which are highly vulnerable to intense sheet and rill erosion processes. The field is managed under conventional tillage with crop rotation; during the year of investigation, the primary crop was sunflower. The field features Luvisols (brown forest soils with clay illuviation) and Colluvisols (colluvial slope sediments) derived from their erosion.

Materials and methods

Tools and softwares

The methodological foundation of the soil loss modeling was the Unit Stream Power-based Erosion Deposition (USPED) model. Its application allowed the classical limitations of the USLE approach to be overcome by accounting for the impact of rill erosion during sediment transport modeling within a two-dimensional flow domain (Mitasova et al. 1996).
As a framework for model parametrization, a Digital Elevation Model (DEM) was generated. A DJI Mavic 3M drone (DJI, Shenzhen, China) was selected for this task because neither alternative freely available or commercial datasets, nor elevation data derived from agricultural machinery logs, are suitable for detecting fine rill erosion features. The orthomosaic was cost-effectively generated at a premium quality using Pixpro software (Pixpro UAB, Vilnius, Lithuania). Subsequently, all necessary spatial computations were performed within the Hydrology toolset of the ArcGIS Pro (Esri, Redlands, CA, USA) Spatial Analyst module. Statistical analyses were executed within a Visual Studio Code environment (Microsoft Corporation, Redmond, WA, USA).

Runoff model generation

To model a continuous, uninterrupted flow network, hydrological correction of the raw UAV-derived DEM was essential using the Fill algorithm. This tool eliminates closed, sink depressions resulting from interpolation noise or micro-topographic irregularities (Wang and Liu 2006).
This topologically consistent surface serves as the foundation for all subsequent cell-level hydrological and soil loss calculations. From the hydrologically corrected DEM, the Flow Direction raster was derived using the deterministic eight-directional (D8) algorithm, which defines surface flow vectors by discretely coding the steepest slope gradients. This direction matrix defines the cell-to-cell topological pathway of gravity-driven runoff across the investigated sub-catchment.
Using the Flow Accumulation algorithm on the Flow Direction matrix, the cell-level calculation of the specific contributing area was performed. The statistically extremely high values precisely delineated the pathways of linearly concentrating surface runoff. This hyper-resolution flow accumulation layer enabled the precise identification of the critical erosion rill, directly guiding the optimal spatial placement of the NbS grassed buffer strip.
Slope angles, which fundamentally dictate the transport capacity and the LS-factor of the USPED model, were computed using the Slope tool based on elevation differences between neighboring cells. The resulting degree values were subsequently converted to radians, as the built-in trigonometric functions of ArcGIS Pro interpret only radian inputs during raster calculator operations.

Hydrological delineation and spatial validation of the sub-catchment

To filter out micro-morphological and tillage noise from the sub-meter resolution slope raster, an Interquartile Range (IQR) filtering protocol was executed on the vectorized point cloud. The spatial continuity of the cleaned data points was restored using Inverse Distance Weighting (IDW) interpolation, creating a smooth terrain surface that accurately reflects true geomorphological slope gradients (Hengl and Reuter 2008).
The outlet (pour point) of the critical erosion rill identified from the Flow Accumulation matrix was snapped to the center of the flow axis using the Snap Pour Point tool. Then, the Watershed tool was executed to delineate the exact sub-catchment area feeding the buffer zone. The topological integrity and boundaries of the hydrologically delineated sub-catchment were cross-verified using an independent spatial validation workflow based on Euclidean distance modeling.

Cell-level grid generation

Finally, for the cell-by-cell USPED computation, a 1×1 m resolution grid was superimposed over the study area. To ensure reproducibility, grid generation and data integration workflows were fully automated using Python-based (ArcPy) scripting. Cell values from the slope and flow accumulation rasters were integrated into the grid attribute table using zonal statistics, establishing a database for the cell-level quantification of the LS-factor and net soil loss (A) (Mitasova et al. 1996).

Results

Soil profile excavation in the upper zone of the sub-catchment

A severely truncated Luvisol (brown forest soil with clay illuviation) profile reflecting intense water and tillage erosion was exposed in the source zone of the rill (Fig. 1). Due to the complete absence of the original, undisturbed humic horizons, the tilled topsoil (Ap, 0–0.3 m) directly overlies a reddish-brown, illuvial clay-accumulation horizon (Bt, 0.3–0.5 m), which transitions into the undisturbed loess parent material (Ck) below 0.5 m.

Fig. 1 Soil profile excavation in the upper zone of the sub-catchment

Soil profile excavation in the lower zone of the sub-catchment

In the lower zone of the rill, a Colluvisol (colluvial slope sediment soil) profile was excavated, exhibiting intense sedimentation and clay accumulation (Fig. 2). The presence of a 1.15 m thick layer of fresh, stratified colluvial sediment (Ap, Ak, 2Ak) fully validates the depositional predictions of the USPED model. The fossil topsoil layer from before the onset of intensive mechanized agriculture (3Ak, 1.15–1.4 m) was found completely buried above the loess parent material (Ck).

Fig. 2 Soil profile excavation in the lower zone of the sub-catchment

In situ determination and evaluation of saturated hydraulic conductivity

Saturated hydraulic conductivity was determined in situ using a constant-head double-ring infiltrometer, where the outer buffer ring minimized lateral flow to ensure strictly vertical infiltration (Jakab et al. 2019; Wischmeier and Smith 1978). Based on the measurements, the truncated erosion zone fell into the most unfavorable class 6 (very slow infiltration) on the Wischmeier scale, which triggers immediate surface runoff and sediment mobilization. Conversely, the accumulation zone exhibited a class 3 (moderate) permeability, confirming a significantly higher water intake and moisture-retention capacity.

Chemical laboratory results

The chemical laboratory analytics (Table 1.) further validated the selective transport mechanism of the finest soil fractions. Due to the selective erosion of colloids and organic matter from the upper zone, the Arany-type stickiness index (KA) increased from 42 to 45 in the lower accumulation zone, while the organic matter (humus) content rose from 2.42% to 3.36%, and the colloid-bound P2O5 concentration enriched from 438 mg kg^{-1} to 626 mg kg^{-1} (Berhe et al. 2018; Stefanovits et al. 2014). Concurrently, the exceptionally high iron (Fe: 194 mg kg^{-1} vs. 105 mg kg^{-1}) and magnesium concentration (327 mg kg^{-1}) of the upper sample chemically confirmed the morphological truncation of the upslope soil. It indicates that tillage operations are already mixing the deeper, iron-oxide and clay-mineral rich illuvial Bt horizon into the current plow layer, proving that homogeneous, field-scale nutrient management is unsustainable.

Table 1. Chemical laboratory analytical results of the 0–0.3 m layer for the lower and upper soil profiles

Sample identifier	pH (KCl)	KA	Humus (%)	$CaCO_3$ (%)	P_2O_5 (mg kg⁻¹)	K_2O (mg kg⁻¹)	Na (mg kg⁻¹)	Mg (mg kg⁻¹)
Upper zone of the sub-catchment	6.05	45	3.36	1.8	626	290	26.1	291
Lower zone of the sub-catchment	6.75	42	2.42	0.659	438	326	18.7	327

Sample identifier	NO_2+ NO_3- N (mg kg^{-1})	S/SO_4- S (mg kg^{-1})	Zn (mg kg^{-1})	Cu (mg kg^{-1})	Mn (mg kg^{-1})	Fe (mg kg^{-1})	Total salt (%)
Upper zone of the sub-catchment	39.2	17.1	6.37	3.51	>200	105	0.072
Lower zone of the sub-catchment	26.5	9.06	4.68	3.24	>200	194	0.045

Mechanical laboratory results

The laboratory texture analysis data (Table 2.) provide direct evidence of downslope mechanical particle sorting and colluvium formation. Easily detachable fine clay particles are transported from the hilltop without deposition, which is reflected in the lower clay content of the upper profile. As the kinetic energy of the surface runoff drops upon hitting the buffer strip boundary, the heavier sand particles deposit first in large volumes, while the dense grass also filters out the finer soil colloids, proving that the buffer strip acts as a highly efficient sediment trap within the catchment system.

Table 2. Mechanical grain-size distribution analysis of the 0–0.3 m layer for the lower and upper soil profiles

Sample identifier	Clay (%)	Silt (%)	Sand (%)	Texture
Upper zone of the sub-catchment	16.89	25.77	57.34	Sandy loam
Lower zone of the sub-catchment	10.31	41.21	48.48	Loam

Calculation of individual factors of the soil loss model

The following equation of the USPED model serves as the computational basis for calculating cell-by-cell soil loss values (Equation 1)

$$A = R * K * LS * C * P \quad (1)$$

where *A* is the average annual soil loss, *R* is the rainfall erosivity factor, *K* is the soil erodibility factor, *LS* is the topographic factor, *C* is the cover and management factor, and *P* is the support practice factor.
The rainfall erosivity factor (R) is based on georeferenced Hungarian Meteorological Service (OMSZ) data. Calculations were performed for both a 2-year return period (R = 875) and a 20-year return period (R = 2040) extreme rainfall event.
Instead of subjective nomograms, soil erodibility (K) was computed from laboratory texture and organic carbon data using the advanced EPIC (Erosion Productivity Impact Calculator) algorithm (Equation 2).

$$K_{us} = (0.2 + 0.3 * e^{-0.0256 * SAN * (1 - SIL/100)}) * (SIL / (CLA + SIL))^{0.3} * (1.0 - (0.25 * OC) / (OC + e^{3.72 - 2.95 * OC})) \quad (2)$$

where K_{us} is the soil erodibility factor calculated using the EPIC model, *SAN* is the sand fraction content, *SIL* represents the silt fraction content, *CLA* is the clay fraction content, *OC* is the organic carbon content of the soil, and *e* denotes the base of the natural logarithm.

The topographic factor (LS) was calculated from the drone-derived DEM using the two-dimensional normalized equation (Moore and Burch 1986; Mitasova et al. 1996) (Equation 3).

$$LS = (m + 1) * (A / 22.13)^{m} * (\sin \beta / 0.0896)^{n} \quad (3)$$

where LS is the topographic slope length and steepness factor, m (m=0.5) is the exponent controlling the sheet erosion component, A represents the specific contributing area or upslope drainage area per unit contour length, beta denotes the slope angle in radians, and n is the exponent reflecting the rill erosion sensitivity (n=1.3).

The cover-management factor was fixed at an average value of C=0.28 based on the crop rotation, and due to the total absence of active contour farming, the support practice factor was defined as a constant P=1.

Potential soil loss and buffer strip deposition efficiency results

Based on the unique values of the 35,922 individual cells (Fig. 3), the potential soil loss of the 3.51 ha sub-catchment area protected by the grassed strip (Fig. 4) would be 85.98 t ha^{-1} (24.50 t ha^{-1} yr^{-1}) under a business-as-usual scenario without protection. This value multiple times exceeds the tolerable soil loss threshold (T-value) established in Europe as balanced with natural soil formation (Panagos et al. 2015; Verheijen et al. 2009). The 4.5 m wide precision grassed strip integrated into the flow accumulation axis provided a 25.4% sediment deposition efficiency based on the non-linear exponential saturation model. Depending on the local rainfall intensity, it retained 21.84 t ha^{-1} of sediment within the field during a 2-year return period event, and 52.41 t ha^{-1} during a 20-year return frequency extreme cloudburst (Yuan et al. 2009) (Equation 4).

$$TE = TE_{max} * (1 - e^{-k * w}) \quad (4)$$

where *TE* is the trapping efficiency of the vegetative filter strip, TE_{max} represents the maximum potential trapping efficiency under ideal conditions, *e* denotes the base of the natural logarithm, *k* is the empirical calibration coefficient determining the extraction rate, and *w* represents the width of the vegetative filter strip.

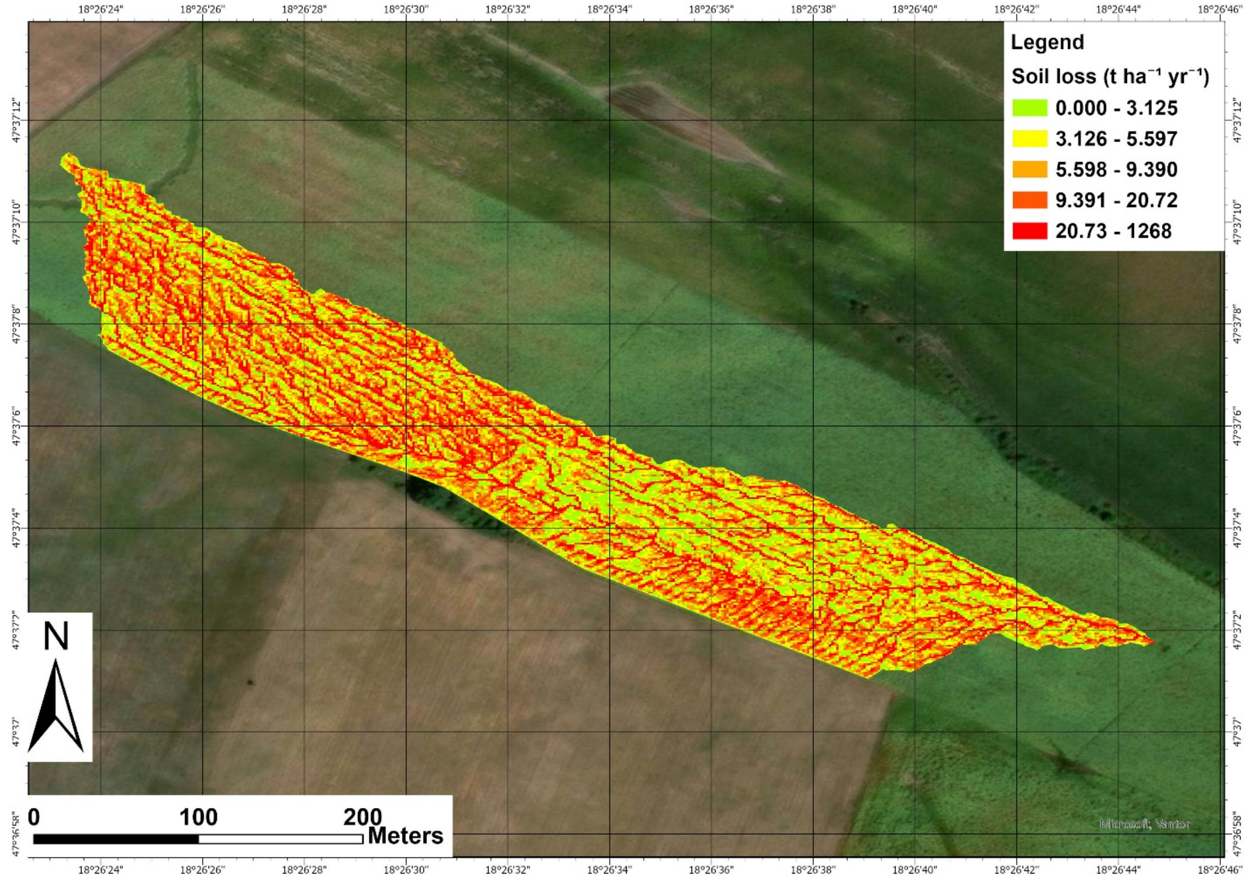

Fig. 3 Soil loss model of the buffer strip sub-catchment

Fig. 4 The implemented grassed buffer strip within the field during sunflower blooming

Correlation analysis

A cell-by-cell statistical correlation analysis revealed that the Spearman rank correlation between net soil loss (A) and flow accumulation showed a stronger positive monotonic relationship (R=0.8634) than the linear Pearson correlation coefficient (R=0.7613). This discrepancy mathematically confirms that the relationship between the variables is non-linear and follows a power function trend. This means that as the contributing drainage area grows, soil loss escalates at an accelerated, non-proportional rate. The descriptive equation is presented below (Equation 5).

$$A = 0.0002 * (Flow\_accu)\text{\^{}}0.4971 \quad (5)$$

where *A* is the potential soil loss, *Flow_accu* represents the flow accumulation value derived from the digital elevation model.

The scaling exponent of 0.4971 provides decisive hydrodynamic evidence: it proves that within the studied sub-catchment, diffuse laminar sheet erosion is heavily outmatched by highly concentrated, turbulent rill and gully erosion processes along the primary flow paths (Govers 1990).

Discussion

Through this hyper-resolution geospatial modeling approach, the primary objective was to validate the real-world applicability and academic scientific merit of process-based soil conservation planning using a multi-tiered validation workflow.

Raw, sub-meter digital elevation models derived from UAV photogrammetry cannot be directly fed into erosion equations due to extensive micro-morphological noise from tillage operations (such as soil clods and tractor data), which yield artificial, extreme local slope gradients (Hengl and Reuter 2008). The multi-step IQR-filtering and IDW-interpolation protocol executed in this study effectively eliminated these high-frequency errors. This fine-tuned, hydrologically sound DEM terrain surface allowed the actual catchment-scale runoff dynamics to be mapped.

The fact that the cell-level Spearman rank correlation coefficient (R=0.8634) markedly outperformed the linear Pearson value (R=0.7613) demonstrates that the relationship between topography and soil loss is fundamentally non-linear in this hilly landscape. The power-law regression exponent serves as hydrodynamic proof that rill and concentrated channelized flows dominate the catchment over uniform sheet wash (Govers 1990). This accelerated progression explains why uniform, field-scale management is structurally flawed, and provides strong scientific justification for why precision, locally targeted interventions along the flow accumulation axes are superior to traditional field-boundary filter strips.

The predicted transport and deposition trends are fully supported by the pedological and laboratory findings. The extremely slow infiltration rates (Wischmeier class 6) of the truncated upper zone trigger immediate surface runoff during intense convective storms. This runoff selectively strips away the most valuable, easily transportable organic colloids and nutrients. While the deposition zone features better hydraulic conductivity, field history shows that without protection, this valley floor regularly suffered from 1–2 hectares of stagnant water bodies after major rainfall events. During the experimental period, local rain gauges recorded 1.04 m of cumulative precipitation. Due to the runoff-attenuating and velocity-breaking properties of the NbS grassed strip, stagnant water ponding was eliminated. This directly protected the sunflower root system from prolonged anoxia, directly contributing to the premium field-average yield of 3.97 t ha^{-1} (Szabó et al. 2020).

Implementing this geospatial soil conservation workflow is highly justified in hilly arable landscapes. High-resolution UAV surveys, professional data processing, and hydrologic design can be readily performed by specialized service providers. Furthermore, the practical establishment of this precision grassed zones can be executed using the existing machinery parks of most commercial farms, requiring minimal land withdrawal and negligible capital expenditure.

Conclusion

Based on the research findings, three structural recommendations are formulated that point toward sustainability, are feasible in practice, and represent the interests of commercial growers.

Instead of rigid, inaccurate, and static estimations, sub-decimeter UAV remote sensing and GIS modeling must become the default management standard for erosion-prone fields, thereby establishing precision soil conservation (Milics 2015).

Due to downslope transport processes, fertilizer application must be strictly adjusted to the topography using Variable Rate Application (VRA) technologies, preventing the washout of input materials applied to erosion zones and the resulting economic losses (Milics 2015).

The development of a complex subsidy system is proposed instead of the current static framework, which recognizes, incentivizes, and supports the ecosystem services of nature-based solutions (Pe'er et al. 2020).

References

Berhe, A. A., Barnes, R. T., Six, J., & Marín-Spiotta, E. (2018). Role of soil erosion in biogeochemical cycling of essential elements: Carbon, nitrogen, and phosphorus. *Annual Review of Earth and Planetary Sciences*, 46(1), 521–548.

Centeri, Cs., Jakab, G., & Kertész, Á. (2019). Sheet erosion. In Á. Kertész (Ed.), *Landscape degradation in Hungary* (pp. 15–24). Budapest, Hungary: Geographical Institute, Research Centre for Astronomy and Earth Sciences.

Govers, G. (1990). Empirical relationships for rill hydraulics and rill erodibility. *Earth Surface Processes and Landforms*, 15(6), 537–546.

Hengl, T., & Reuter, H. I. (Eds.). (2008). *Geomorphometry: concepts, software, applications*. Amsterdam, Netherlands: Elsevier.

Jakab, G., Szalai, Z., Kertész, Á., Tóth, A., Madarász, B., & Szabó, J. A. (2019). Talajeróziós folyamatok vizsgálata és modellezése magyarországi mintaterületeken (Investigation and modeling of soil erosion processes in Hungarian study areas). *Földrajzi Közlemények*, 143(2), 112–126.

Milics, G. (2015). A precíziós növénytermesztés térinformatikai és technológiai alapjai (Geoinformatics and technological bases of precision crop production). *Agrárelőrejelzés*, 4(1), 22–31.

Mitasova, H., Hofierka, J., Zlocha, M., & Iverson, L. R. (1996). Modelling topographic potential for erosion and deposition using GIS. *International Journal of Geographical Information Systems*, 10(5), 629–641.

Moore, I. D., & Burch, G. J. (1986). Physical basis of the length-slope factor in the Universal Soil Loss Equation. *Soil Science Society of America Journal*, 50(5), 1294–1298.

Panagos, P., Borrelli, P., Poesen, J., Ballabio, C., Lugato, E., Meusburger, K., et al. (2015). The new assessment of soil loss by water erosion in Europe. *Environmental Science & Policy*, 54, 438–447.

Pe'er, G., Bonn, A., Bruelheide, H., Dieker, P., Eisenhauer, N., Feindt, P. H., et al. (2020). Action needed for the EU Common Agricultural Policy to deliver on sustainability. *People and Nature*, 2(2), 305–316.

Stefanovits, P., Filep, Gy., & Füleky, Gy. (2014). *Talajtan (Soil Science)*. Budapest, Hungary: Mezőgazda Kiadó.
Szabó, B., Weynants, M., & Tóth, B. (2020). Mapping soil hydraulic properties at regional scale using pedotransfer functions. *Geoderma*, 365, 114213.
Verheijen, F. G., Jones, R. J., Rickson, R. J., & Smith, C. J. (2009). Tolerable soil loss in Europe: a state-of-the-art review. *Earth-Science Reviews*, 96(1-2), 22–38.
Wang, L., & Liu, H. (2006). An efficient method for identifying and filling depressions in digital elevation models. *International Journal of Geographical Information Science*, 20(2), 193–213.
Wischmeier, W. H., & Smith, D. D. (1978). *Predicting rainfall erosion losses: a guide to conservation planning* (Agriculture Handbook No. 537). Washington, DC, USA: Science and Education Administration, United States Department of Agriculture.
Yuan, Y., Bingner, R. L., & Locke, M. A. (2009). A review of effectiveness of vegetative buffers on sediment traps in agricultural watersheds. *Journal of Environmental Sciences*, 21(9), 1211–1219.